Liposome-Mediated Radiotherapeutics Within Avascular Tumor Spheroids: Comparative Dosimetry Study for Various Radionuclides, Liposome Systems, and a Targeting Antibody

Dimitris Emfietzoglou, PhD[1]; Kostas Kostarelos, PhD[2]; Alexandros Papakostas, MSc[1]; Wei-Hong Yang, MD[3]; Åse Ballangrud, PhD[3]; Hong Song, PhD[4]; and George Sgouros, PhD[4]

[1]Department of Medical Physics, University of Ioannina Medical School, Ioannina, Greece; [2]Centre for Drug Delivery Research, The School of Pharmacy, University of London, London, United Kingdom; [3]Department of Medical Physics, Memorial Sloan-Kettering Cancer Center, New York, New York; and [4]Department of Radiology, Johns Hopkins University, School of Medicine, Baltimore, Maryland

Absorbed dose profiles within tumor spheroids simulating avascular micrometastases have been calculated for a variety of liposome- and antibody-radionuclide combinations to assess the anticipated therapeutic efficacy based on the intratumoral distribution of the carrier systems within the spheroid model. **Methods:** Experiments studying the targeting and diffusion capability of the most clinically relevant liposome systems and the anti-PSMA (prostate-specific membrane antigen) antibody J591 within spheroids of the prostate cancer cell line LNCaP (diameter, 150–200 μm) have been performed. The intratumoral biodistribution data were then used as the input to obtain absorbed dose profiles within the tumor spheroid mass. The dosimetric analysis was performed for a variety of medium- and high-energy β-emitting radionuclides (^{32}P, ^{90}Y, ^{188}Re, ^{67}Cu, ^{131}I) and 2 low-energy Auger or conversion electron emitters (^{123}I, ^{125}I) following the point-kernel convolution method in the continuous slowing-down approximation. **Results:** Relative absorbed dose distribution calculations as a function of the distance from the rim of the spheroids are presented. For all liposome systems studied, the SUV-DMPC-chol (small unilamellar vesicle–dimyristoyl-phosphatidylcholine–cholesterol) was most efficient in penetrating deeper within the spheroids. For the β-emitters it delivered its maximum absorbed dose (D_{max}) at 40- to 50-μm depth, exhibiting an almost flat absorbed dose profile beyond that point, as is evident by the high absorbed dose value at the center of the spheroid (D_{core}), $D_{core}/D_{max} > 0.9$; the respective values for the J591 antibody were 20 μm and 0.85. The Auger or conversion emitters resulted in the most heterogeneous absorbed dose distribution; the ratio D_{core}/D_{max} fell to 0.4 for the SUV-DMPC-chol and to 0.4–0.5 for the antibody. In general, a 2- to 10-fold "cross-fire"–related increase of the core absorbed dose was observed. For liposomes exhibiting high binding capacity (3β-[*N*-(*N′*,*N′*]-dimethylaminoethane)carbamoyl]cholesterol [DC-chol]), however, the low-energy emitters deliver up to a 40% higher D_{max} relative to the β-emitters. The surface characteristics of liposomes appear to have a noticeable influence on the absorbed dose profiles. The use of neutral (DMPC-chol) versus cationic (DC-chol) lipids resulted in up to a 10-fold increase of D_{core}/D_{max} depending on the radionuclide. Changing the cationic lipid used to *N*-[1-(2,3-dioleoyloxy)propyl]-*N,N,N*-trimethylammonium methyl sulfate also had a notable influence (up to a 6-fold increase), whereas the effect of fusogenic lipids (dioleoylphosphatidylcholine) was found to be much smaller. **Conclusion:** It is possible to engineer liposome systems that are particularly effective in delivering an almost uniform absorbed dose profile at the central region of micrometastatic tumors, provided that conjugates with the appropriate radionuclides are constructed. In view of the passive means of diffusion of liposomes within solid tumors, it is suggested that they may effectively complement an antibody-based therapeutic regime against micrometastatic tumors, leading to cytotoxic absorbed dose levels throughout the entire tumor volume—thus, hindering tumor recurrence.

Key Words: radiotherapeutics; dosimetry; liposome systems; radiotherapy; radionuclides; spheroids

J Nucl Med 2005; 46:89–97

The construction and use of liposome systems as targeted delivery vehicles of therapeutic agents has mainly focused on enhancing the tumor-to-blood concentration ratio of the delivered therapeutic (*1,2*). In a previous study we undertook a first-order dosimetric evaluation for the use of liposomes in radiotherapeutic applications based on whole-organ and blood biodistribution data (*3*). It was shown that particular liposome systems provide adequate targeting efficiency to solid tumors when combined with radionuclides of specific emission characteristics. Importantly, unlike radioimmunotherapy, in which the red marrow is dose limiting, the dose-limiting organ in such applications appeared to be the liver, which can tolerate considerably larger absorbed doses than the marrow.

Received Mar. 4, 2004; revision accepted Aug. 17, 2004.

For correspondence or reprints contact: George Sgouros, PhD, Department of Radiology, Johns Hopkins University, School of Medicine, 720 Rutland Ave., Baltimore MD 21205.

E-mail: gsgouros@jhmi.edu

The clinical application of radiolabeled liposomes, or any other tumor-targeting moiety, is faced with the problem of insufficient penetration and, thus, inhomogeneous distribution within the tumor volume (*4*). This is one of the main obstacles to the effective application of radiolabeled antibodies in the treatment of bulky disease (*5*). Toward internal radiotherapy of micrometastasis, on the other hand, many of the obstacles associated with the treatment of bulky disease—extravasation from tumor microvasculature, interstitial diffusion, and tumor penetration—are less of a concern (*6*). This realization presents a compelling rationale for targeting disseminated tumor cell clusters using radiolabeled monoclonal antibodies (*7*). In this case, the emission characteristics of the radionuclides will be more critical due to the small dimensions of the tumor (<1 mm) involved, which may reach the single-cell limit (*8–10*). However, the ability of any radiolabeled carrier to deliver a uniform absorbed dose profile throughout the entire target volume with minimal irradiation of the surrounding healthy tissues still remains an important factor (*11,12*).

Previously, we studied the absorbed dose–response profiles of monoclonal antibody–targeted radionuclides toward development of radioimmunotherapeutics against prostate carcinomas (*13*). The avascular multicellular spheroid model for a prostate carcinoma cell line (LNCaP) was used in those studies (*14*). Other investigators have also studied absorbed dose–response curves for external (*15*) and internal (*16–18*) radiotherapeutic regimes using tumor spheroid models of various carcinomas. Moreover, satisfactory correlation was found between the absorbed dose–response profiles and tumor growth curves obtained in vitro using the LNCaP spheroid model. Improved overall survival and significant reduction of prostate-specific antigen (PSA) blood levels in an intramuscular xenograft model of LNCaP cells, when treated with an α-particle–emitting radioimmunoconjugate, have also been reported (*19*). Contrary to the extensive studies previously evaluating monoclonal antibody-radioconjugates for cancer radioimmunotherapy, liposomes have only recently been proposed and evaluated as delivery systems of radiotherapeutic agents (*3,20,21*).

The present work presents a comparison of absorbed dose profiles within avascular prostate carcinoma spheroids of the LNCaP cell line for various β-emitters and Auger or conversion electron emitters delivered by liposomes and a monoclonal antibody. Experimental studies for the binding and diffusion of the most clinically relevant liposome systems within the spheroids have been performed and used as the input to the dosimetric model. Similar data for the anti-PSMA (prostate-specific membrane antigen) antibody J591 have been produced for comparison. The cell line characteristics and spheroid dimensions used in this study are mostly relevant to avascular prostate micrometastasis in vivo.

MATERIALS AND METHODS

Spheroids

Multicellular spheroids consisting of the LNCap-LN3 prostate tumor cell line were prepared according to the liquid overlay technique of Yuhas et al. (*22*) as described in detail previously (*14*). Approximately 10^6 LNCaP-LN3 cells, obtained by trypsinization from growing monolayer cultures, were seeded into 100-mm dishes coated with a thin layer of 1% agar (Bacto Agar; Difco) with 15 mL of RPMI 1640 medium, supplemented with 10% fetal bovine serum, 100 units/mL penicillin, and 100 μg/mL streptomycin. After 3–5 d in the agar culture, spheroids of 200 ± 400 μm in diameter were selected under an inverted phase-contrast microscope with an ocular scale using an Eppendorf pipette. The selected spheroids were transferred to 35-mm bacteriologic Petri dishes in 2 mL of medium.

Liposomes

The most relevant liposome systems for clinical applications were constructed and used in the present study. Liposomes were prepared as multilamellar vesicles (MLVs) and small unilamellar vesicles (SUVs), differing in the mean particle size of the respective liposome populations. Light and electron microscopy indicated that the mean vesicle diameter for all MLV systems ranged between 800 and 1,000 nm and for all SUV systems this diameter ranged between 50 and 150 nm, whereas the total lipid composition for both systems was kept constant at 1 mg/mL. Liposomes were prepared following the solvent evaporation–hydration protocol, by solubilization of all lipids into laboratory-grade chloroform (United States Pharmacopeia) and subsequent evaporation under high pressure to form a lipid film. Hydration of the lipid films, by addition of either phosphate-buffered saline (PBS) (in experiments not involving cells) or RPMI medium (for cellular experiments), produced MLVs. Extrusion cycles through polycarbonate filters (Millipore) using a manual extruder (Avanti Polar Lipids) was used to form SUVs according to a previously described protocol (*23*). A constant concentration (3.75 μg/0.5 mg lipid) of the lipophilic carbocyanine dye 1,1′-dioctadecyl-3,3,3′,3′-tetramethylindocarbocyanine perchlorate (DiI), which has been shown to be an efficient liposome bilayer marker for in vivo localization studies (*24*), was used for labeling.

The surface characteristics, in terms of surface charge and bilayer properties, of both MLV and SUV liposomes were varied using dimyristoyl-phosphatidylcholine (DMPC), 3β-[*N-(N′,N′*-dimethylaminoethane)carbamoyl]cholesterol (DC-chol), and cholesterol (chol), purchased from Sigma, and *N*-[1-(2,3-dioleoyloxy)propyl]-*N,N,N*-trimethylammonium methyl sulfate (DOTAP), purchased from Avanti Polar Lipids. The surface properties of the liposomes were evaluated using a DELSA 440 Zetasizer instrument (Beckman-Coulter). The liposome systems studied along with their surface characteristics are presented in Table 1.

Antibodies

The anti-PSMA antibody (J591) targets the external domain of PSMA expressed on the surface of the LNCaP cells at a density of about 180,000 sites per cell (*25,26*). Using a modified Scatchard analysis, an antigen site density for the LN3 subline of 130,000 sites per cell was measured (*27*). PSMA expression has also been found in tumor but not in normal vascular endothelium (*25,28*). Fluorescein isothiocyanate (F7250; Sigma Chemical Co.) (FITC)-

TABLE 1
Liposome Systems

Liposome system (molar ratio)	Surface charge (mV)	Bilayer characteristics (at 37°C)
DMPC:chol (2:1)	−9.3 ± 2.2	LQ
DMPC:DC-chol (2:1)	51.7 ± 3.9	LQ
DMPC:DOPE:DC-chol (2:1:0.5)	55 ± 6.7	LQ/fusogenic
DMPC:DOPE:DOTAP (2:1:0.5)	49 ± 5.0	LQ/fusogenic

LQ = liquid crystalline.

conjugated J591 was used to fluorescently label the antibody as described previously (*13*).

Experimental Protocol

Multicellular spheroids were coincubated with the various liposome systems for 2, 5, and 24 h at 37°C before confocal laser scanning microscopy. All incubations were undertaken in an orbital shaker incubator. For the antibody experiments the spheroids were incubated with FITC-conjugated J591 for 2, 3, 18, and 24 h. Because no appreciable changes were observed between the 2 last time points for both the liposome systems and the antibody, further measurements beyond 24 h were not performed. Five spheroids were studied in each condition. Before imaging, spheroids were washed 3 times with PBS and placed in their incubation medium. Confocal laser scanning fluorescence microscopy (Zeiss LSM 510; Carl Zeiss, Inc.) was performed by acquiring 3-μm-thick optical sections of the spheroids under study from the top toward the center of the spheroids, until scanning ~120 μm deep into the spheroid. The fluorescence profile of each spheroid as a function of depth was determined from the average intensity along 50 equally spaced spheroid diameters using the image analysis software Intelligent View (version 1.2 by Bokwon Yoon). For each spheroid image, the obtained radial profiles were corrected for background fluorescence as well as for the exponential light attenuation due to scattering and absorption within the spheroid. The linear attenuation coefficient was determined in separate experiments from spheroids of cells transfected with a fluorescent protein (*13*).

Radionuclides

The selection of a radionuclide should account for both the particular size of the tumor mass targeted and the delivery system kinetics within the tumor. In general, high-energy electrons (hundreds of kiloelectron volts) are required for bulky tumors (diameter > 1 cm), whereas, medium- and low-energy electrons should be more appropriate for small tumors and a cluster of cells, respectively, to spare the surrounding normal tissues. Of course, the extent of low-dose or unirradiated regions, due to the nonuniform diffusion of the carrier, will be decisive in the determination of the optimum electron range (and energy) (*12*). Similarly, short-lived radionuclides (half-life < 1 d) may be optimum for hematologic tumors, which may be rapidly targeted, whereas a half-life of a few days may be necessary for solid tumors, not easily accessed. Several radionuclides with diverse emission properties were included in the present study. With respect to particle characteristics, both high- and medium-energy β-emitters (^{90}Y, ^{188}Re, ^{32}P and ^{131}I, ^{67}Cu, respectively), as well as Auger and internal conversion electron emitters (^{123}I, ^{125}I), have been used. The half-lives of the radionuclides studied span several hours (^{123}I, ^{188}Re) to days (^{90}Y, ^{32}P, ^{131}I, ^{67}Cu, ^{125}I). The emission properties of the examined radionuclides are presented in Table 2.

Dosimetry

The absorbed dose profiles have been calculated based on electron point-kernels calculated in the continuous slowing-down approximation (CSDA) using the geometric model of Howell et al. (*29*). Note that any photon contribution is negligible for the spheroid dimensions used here. The spheroid was assumed to be a unit density sphere containing a nonuniform, but spherically symmetric, radionuclide concentration. The functional dependence of the radionuclide concentration with respect to the spheroid radius was taken to be identical to the fluorescent profile obtained by the image analysis. Various combinations of Weibull, rational, and inverse polynomial functions were used to fit the fluorescent profiles using the fitting routines of the SigmaPlot software package (SPSS Inc.). The energy spectra of the β-emitters were taken from Cross et al. (*30*) and analytically represented by polynomials of various orders. Electron point-kernels were calculated in the CSDA by means of Cole's energy range relationship (*31*), which is sufficiently accurate above a few tens of kiloelectron volts. Although energy-loss straggling is neglected in this approach, Cole's formula has been established experimentally and, thus, accounts for multiple scattering providing, essentially, the penetration depth, which is really the quantity of interest here (*32*). Absorbed fractions were then calculated by convolution of the radionuclide distribution functions and the point-kernel functions (*31*). In the numeric evaluation of the double integral over, essentially, the slowing-down electron energy and spheroid radius, the continuous β-spectra were divided into energy bins of 10-keV width, whereas the spheroid was divided in concentric shells of 2- to 20-μm width. The 10-keV limit in the initial electron energy was based on the fact that the range of such electrons is about 1 μm and, therefore, a better energy resolution would have been necessary only if subcellular data were available. The lower limit put on the spheroid shell width was chosen to roughly match the 10-keV energy resolution; the 2-μm value was used at depths of high absorbed dose gradient (0- to 30-μm depth), whereas the increase to 20 μm was used at larger depths to speed up the computations. The absorbed dose rate per unit activity was then calculated by summing, in the case of a β-spectrum, over all energy bins with the appropriate weighting factor. In the absence of a calibration of the fluorescent intensity in terms of radionuclide activity, the absorbed dose results are expressed in arbitrary units. Thus, comparisons are made in terms of relative absorbed dose distributions. Finally, since the kinetics of the carrier within the

TABLE 2
Properties of Radionuclides

Radionuclide	Half-life (d)	Mean energy (keV)	Tissue range (mm)
^{125}I	60.14	18	0.007
^{123}I	0.55	28	0.016
^{67}Cu	2.58	141	0.7
^{131}I	8.04	182	0.9
^{32}P	14.3	695	3.0
^{188}Re	0.71	765	3.8
^{90}Y	2.67	934	4.0

spheroids was studied by images taken at discrete time points (e.g., at 2, 5 h, and so forth), each activity profile was assumed "frozen" in-between the midpoints of each time interval. This is a good approximation given that the half-life of the examined radionuclides is much larger than the time required for the liposomes to reach a steady-state concentration profile (~2–5 h), while the kinetics of the antibody appear also not to change drastically beyond 3–5 h. Finally, the total absorbed dose to each shell was obtained by summing the absorbed doses corresponding to each time interval, which, in turn, was calculated by multiplying the frozen activity distribution with the total number of disintegrations taken place at that particular time interval. All numeric calculations were performed using the Mathematica software package (Wolfram Research Inc.).

RESULTS

Fluorescence intensity profiles as a function of distance from the rim of the spheroids for 2 representative liposome systems—namely, a multilamellar (MLV) and a small unilamellar (SUV) liposome (Table 1) as well as for the FITC-labeled antibody (J591) are shown in Figure 1. Intensity has been corrected for background and attenuation, as discussed earlier. For all liposome systems, negligible change in the distribution profile was observed beyond 5 h after incubation and until the 24-h endpoint. Similarly, for the antibody, no appreciable differences between the last 2 time points (18 and 24 h) may be observed. Thus, further measurements beyond 24 h were not performed. The analytic functions obtained by fitting the kinetic data have been used as the input to the dosimetric model.

The degree of uniform distribution of the delivery systems within the spheroids is shown in Figure 2. All profiles have been normalized to their individual peak values. A comparison between various liposome systems is presented in Figure 2A, whereas the normalized profiles for the J591 antibody at each time point are shown in Figure 2B. To facilitate the comparison, the liposome profiles refer to the average values between the 2- and 5-h data points.

Radial absorbed dose profiles within the spheroids are shown in Figure 3. Again, the profiles have been normalized to their individual peak values; the ratio D/D_{max} represents the radial distribution of absorbed dose relative to the maximum absorbed dose value of the distribution. We depict the 2 liposome systems, from the MLV and SUV groups, exhibiting the highest penetration efficiency (DMPC:DOPE:DOTAP and DMPC-chol, respectively, where DOPE = dioleoylphosphatidylcholine), along with the J591 antibody. The results have been obtained by the point-kernel convolution method, as described in the Dosimetry section. The normalized fluorescent data for each carrier system (designated as C/C_{max}), taken from Figures 2A and 2B, is also shown to get an estimate of "cross-fire"–related effects.

The normalized absorbed dose profiles for a low-energy (^{123}I) and a high-energy (^{90}Y) electron emitter are shown in Figure 4. These profiles will not appreciably change if any other low- or high-energy electron emitter is chosen. A comparative assessment of the absorbed dose-uniformity

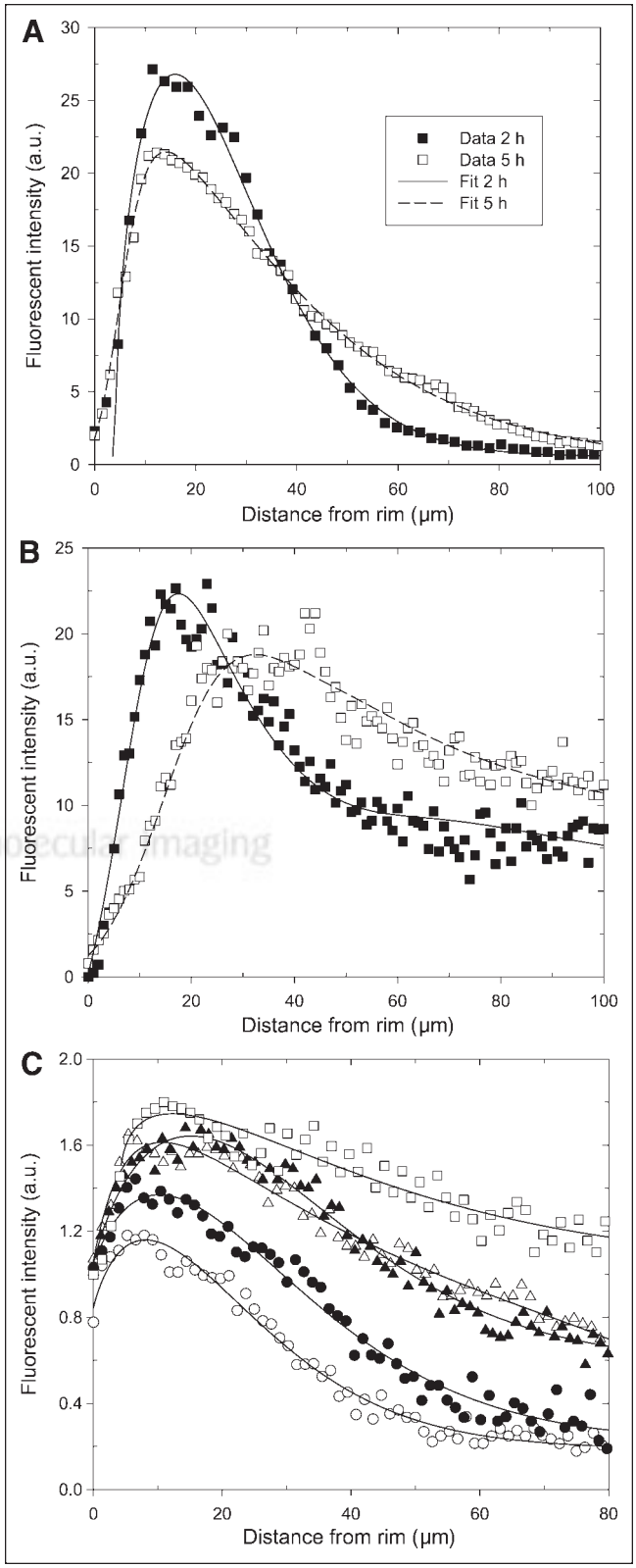

FIGURE 1. Fluorescent intensity profiles in arbitrary units (a.u.) as function of distance from rim of spheroid at various times after incubation for liposome system MLV (DMPC:DOPE:DOTAP, where DOPE = dioleoylphosphatidylcholine) (A), liposome system SUV (DMPC:chol) (B), and antibody J591 (from bottom to top curve: 1, 2, 3, 18, and 24 h) (C).

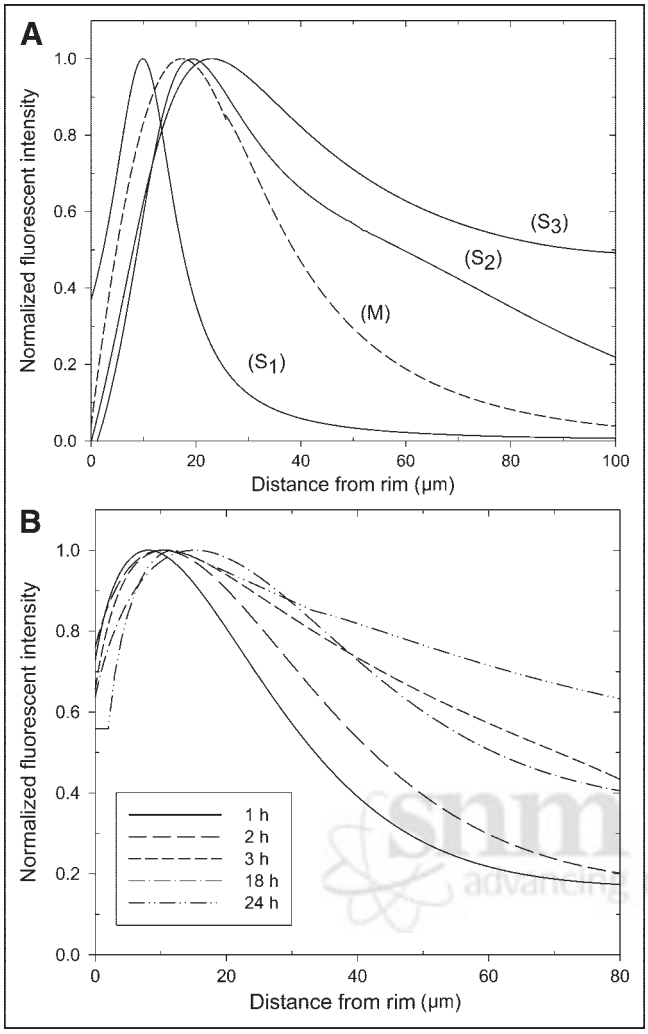

FIGURE 2. Fluorescent intensity profiles normalized to their peak values. (A) Liposome systems (average for 2 time points): S_1 = SUV DMPC:DC-chol; S_2 = SUV DMPC:DOPE:DOTAP (DOPE = dioleoylphosphatidylcholine); S_3 = SUV DMPC-chol; M = MLV DMPC:DOPE:DOTAP. (B) J591 antibody.

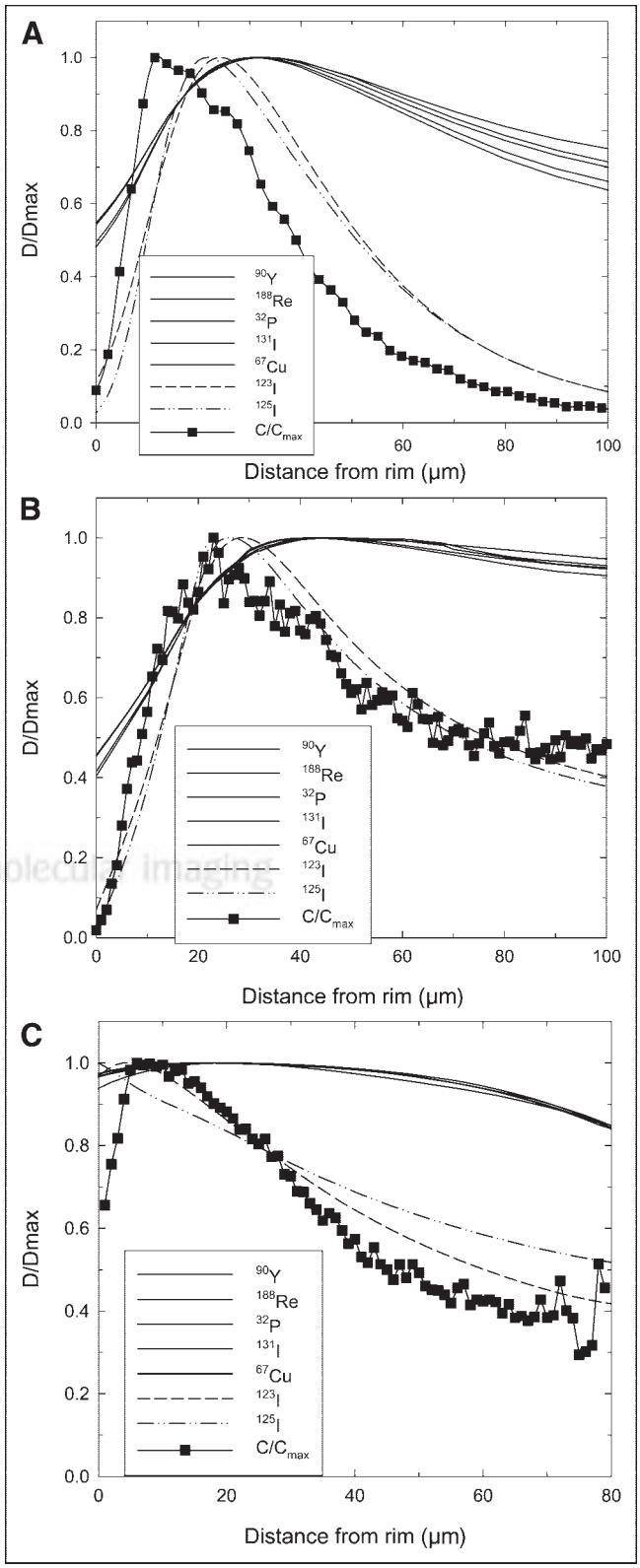

FIGURE 3. Cumulative absorbed dose distribution profiles normalized to the maximum (D/D_{max}) absorbed dose value of the distribution for all electron-emitting radionuclides studied. Boxes are normalized fluorescent profiles of carrier (an average value for all time points was used). (A) MLV (DMPC:DOPE:DOTAP, where DOPE = dioleoylphosphatidylcholine). (B) SUV (DMPC-chol). (C) J591 antibody.

profiles for all radionuclide-carrier combinations examined may be greatly facilitated by the summary of Table 3, which presents the depth (R) of maximum absorbed dose (D_{max}) and the normalized absorbed dose at the core (c) of the spheroid (D_c/D_{max}). Sterilization of tumor cells, however, will depend not only on the distribution of absorbed dose within the tumor volume but also on the ability of the radionuclide-carrier conjugate to deliver high enough absorbed doses to the tumor cells. In Figures 5 and 6 the relative absorbed dose profiles per radionuclide decay and the cumulative absorbed dose profiles, respectively, for the 2 liposome systems are shown for the various electron emitters. The profiles in Figure 5 represent the effect of electron energy (or cross-fire effect), whereas in Figure 6 the half-life of the radionuclide (along with the kinetics of the carrier) becomes most critical. In the present calculation, cumulative absorbed dose profiles have been obtained by

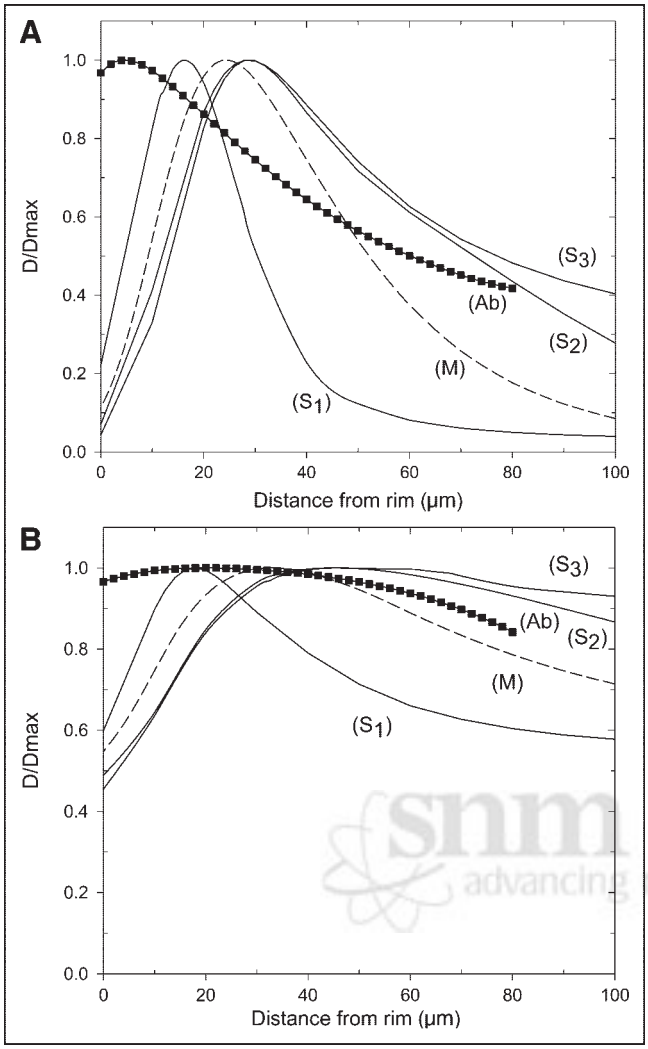

FIGURE 4. Normalized (cumulative) absorbed dose distribution profiles for various carrier systems studied (symbols as in Fig. 2; Ab = antibody) for 2 electron emitters with very different emission characteristics. (A) Low-energy emitter with short half-life: ^{123}I. (B) High-energy β-emitter with long half-life: ^{90}Y.

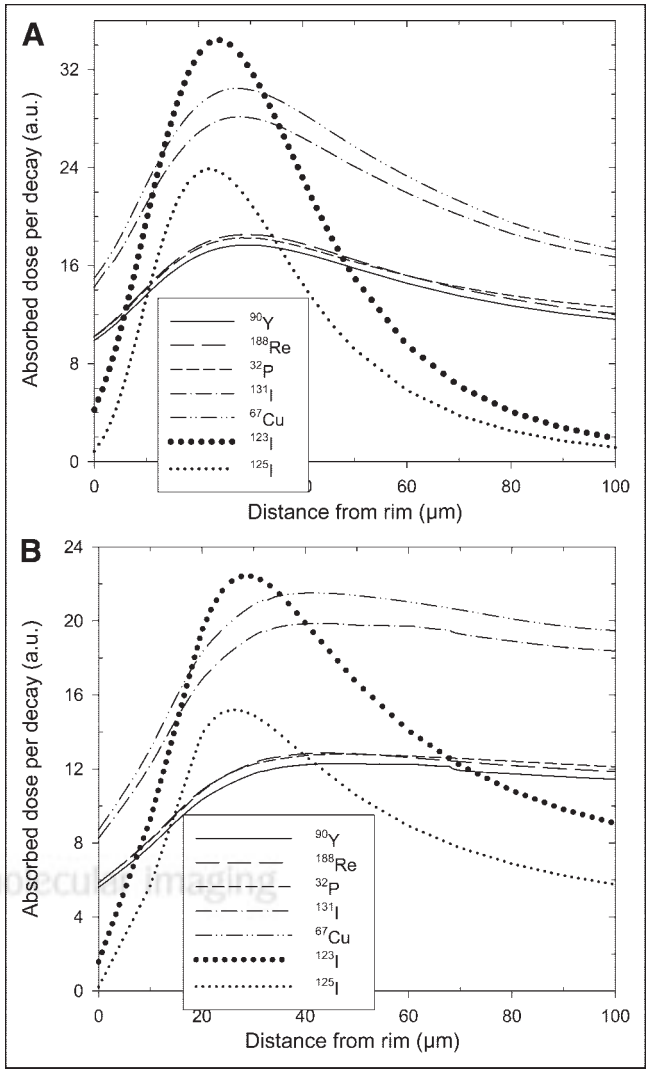

FIGURE 5. Absorbed dose profiles in arbitrary units (a.u.) per radionuclide decay calculated for all radionuclides studied for 2 liposome systems. (A) MLV (DMPC:DOPE:DOTAP). (B) SUV (DMPC-chol).

TABLE 3
Cumulative Absorbed Dose Calculations

Carrier system	^{90}Y		^{188}Re		^{32}P		^{131}I		^{67}Cu		^{123}I		^{125}I	
	R (μm)	D_c/D_{max}	R (μm)	D_c/D_{max}	R (μm)	D_c/D_{max}	R (μm)	D_c/D_{max}	R (μm)	D_c/D_{max}	R (μm)	D_c/D_{max}	R (μm)	D_c/D_{max}
MLV (DMPC:DC-chol)	16	0.62	16	0.62	16	0.65	14	0.55	14	0.52	14	0.05	12	0.04
MLV (DMPC:DOPE:DC-chol)	22	0.69	22	0.68	22	0.72	20	0.62	20	0.59	18	0.07	16	0.06
MLV (DMPC:DOPE:DOTAP)	32	0.71	32	0.70	32	0.75	32	0.66	30	0.64	24	0.09	22	0.09
SUV (DMPC-chol)	46	0.93	44	0.92	48	0.95	42	0.92	42	0.91	28	0.40	26	0.38
SUV (DMPC:DC-chol)	18	0.58	18	0.56	18	0.61	18	0.52	18	0.49	16	0.04	16	0.04
SUV (DMPC:DOPE:DC-chol)	20	0.61	20	0.60	20	0.63	20	0.53	20	0.50	20	0.07	18	0.05
SUV (DMPC:DOPE:DOTAP)	44	0.87	44	0.86	44	0.90	42	0.84	40	0.82	28	0.28	26	0.25
Antibody J591	20	0.84	20	0.85	20	0.84	20	0.84	16	0.85	4	0.42	0	0.52

R refers to distance from rim of spheroid where absorbed dose is maximum (D_{max}); D_c was calculated at core of spheroid, which was at 100-μm depth for liposome experiments and 80-μm depth for antibody.

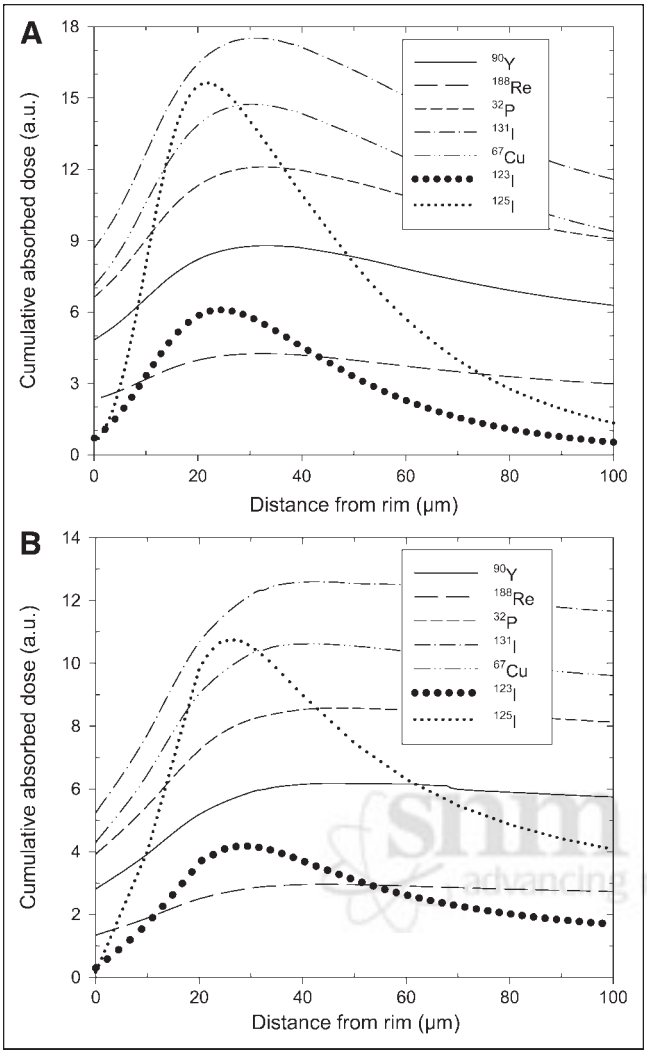

FIGURE 6. Cumulative absorbed dose profiles in arbitrary units (a.u.) calculated for all radionuclides studied for 2 liposome systems. (A) MLV (DMPC:DOPE:DOTAP). (B) SUV (DMPC-chol).

using an approximate upper limit of 3 d, since the spheroids have been shown to undergo structural or geometric changes after a few days following incubation with radiolabeled antibodies (*13*). In general, increasing the upper limit further would result in larger absorbed dose values, especially for the long-lived radionuclides. Given the experimental evidence (*13*), however, the geometric model parameters used in the present dosimetry would have been unrealistic for use at longer times.

DISCUSSION

Therapeutically effective targeting of radiolabeled carrier systems within a tumor mass is determined by the delivery of cytotoxic levels of absorbed dose throughout all viable cells capable of further divisions, without intolerably irradiating the surrounding tissues. However, numerous factors, largely stemming from tumor biology, result in a nonuniform distribution of radioactivity—particularly within solid tumors—which leads to subcytotoxic absorbed doses of radiation to cells residing close to the central region of the tumor (*33*). The latter presents a major obstacle to successful radiotherapy, resulting in hypoxic cells of increased radioresistance (*34*).

In the present study it has been shown that, despite the generally limited diffusion of the carriers within the spheroids, which, in most cases, reached a relative concentration in the core region well below 50% (i.e., the $C_{core}/C_{max} < 0.5$; Fig. 2A), a careful selection of a radionuclide may result in a 2–10 times increase of the respective absorbed dose ratio due to cross-fire–related effects (Table 3). In particular, the SUV-DMPC-chol system exhibited an almost flat absorbed dose profile ($D/D_{max} > 0.9$) beyond the peak depth (at about 40–50 μm) for all β-emitting radionuclides studied, resulting in an almost 2-fold cross-fire increase (Fig. 3B). Similarly, the J591 antibody, which reached about 60% core concentration only after 24 h after incubation (Fig. 2B), exhibited a normalized core absorbed dose exceeding 80% when combined with any of the β-emitters (Table 3)—that is, a 1.4-fold cross-fire increase. As expected, no such effect was observed for the low-energy emitters (^{123}I and ^{125}I) due to their extremely short electron ranges (of cellular dimensions). The pronounced fall of absorbed dose close to the periphery for the liposome systems presented is due to the fact that, as noted in the experimental protocol, the spheroids to be imaged were washed with media to remove any fluorescent signal interference from unbound carriers around the spheroid. As a result, those liposomes that were loosely bound onto the spheroid surface were also removed. This artifact of the washing protocol vanishes for the antibody, where uptake is much more readily occurring, due to the much stronger cell surface interaction and to the weaker hydrostatic forces.

The effect of electron range is most clearly seen by comparison of the results in Figures 4A and 4B, where, for all carrier systems, ^{90}Y delivers a substantially more uniform absorbed dose distribution than ^{123}I. From Figure 4 (and Table 3), it is also evident that the surface characteristics of liposomes have a noticeable influence on the absorbed dose profiles. For example, the use of neutral (DMPC-chol) versus cationic (DC-chol) lipids resulted in up to a 2-fold increase of D_c/D_{max} for the β-emitters and up to a 10-fold increase for the low-energy emitters. Changing the cationic lipid used to DOTAP also had a notable influence (up to a 6-fold increase), whereas the effect of fusogenic lipids (DOPE) was found to be much smaller.

On the other hand, the ratio of tumor-to-normal-tissue absorbed dose would be increasingly lower for the high-energy electron emitters, since a significantly greater proportion of their energy would be deposited outside the tumor volume. In addition, >90% of the tumor volume (i.e., tumor cells) is contained in the outer half of the spheroid. A theoretic analysis by Howell et al. (*29*) has examined these aspects and revealed the importance of low- to medium-energy electron emitters. Even more so, low- to medium-

energy electrons may be more effective in sterilizing the tumor cells by delivering higher absorbed doses due to the inverse proportionality of the linear energy transfer to the electron energy (at the keV range). It is apparent in Figure 5 that the medium-energy β-emitters (^{67}Cu and ^{131}I) deliver about 1.5 times higher absorbed doses per decay than the high-energy β-emitters (^{32}P, ^{188}Re, ^{90}Y). On the other hand, the higher electron energy of ^{123}I over ^{125}I, together with the fact that there is almost complete absorption of their electrons within the spheroid, results in a higher absorbed dose per decay for ^{123}I. The therapeutic effect, however, will depend on the cumulative tumor absorbed dose from all of those radioactive decays resulting in tumor irradiation. It may be seen from Figure 6 that those β-emitters having a combination of longer half-life and lower electron energies are the ones delivering the higher cumulative absorbed doses. Therefore, whereas in Figure 5 the ^{67}Cu was more effective per decay than ^{131}I, due to its softer β-spectrum, the cumulative absorbed dose delivered by ^{131}I is greater than ^{67}Cu, due to its longer half-life. For the same reason, the equivalence in terms of absorbed dose per decay (Fig. 5) observed for the high-energy β-emitters (^{32}P, ^{188}Re, ^{90}Y) has been substituted by the relationship ^{32}P > ^{90}Y > ^{188}Re for the cumulative absorbed dose (Fig. 6). The results for the other carrier systems are similar since the half-lives of the radionuclides are much larger than the kinetics of the carrier systems examined (on the order of hours).

In general, the ideal absorbed dose distribution would be one that accounts for variations in tumor cell radiosensitivity and density of clonogens. In this regard, the ideal absorbed dose distribution across a spheric tumor mass must balance the effects of clonogen density, favoring a greater absorbed dose on the periphery of the tumor, and radiosensitivity, favoring a greater absorbed dose at the core of a tumor, wherein hypoxia-induced radioresistance is likely. For micrometastases of up to 100- to 150-μm radius that lack a hypoxic region, these considerations translate into an absorbed dose profile that, ideally, matches the cell density profile. In such a circumstance, absorbed dose profiles exhibiting a substantially higher surface layer absorbed dose relative to the core might be more appropriate. As noted earlier, when a high absorbed dose to the periphery and to the core is deemed optimal, MLV (DMPC:DOPE:DOTAP) and SUV (DMPC-chol) were found to provide the most uniform absorbed dose distributions, overall. If, however, the response is primarily influenced by clonogen density, then SUV (DMPC:DOPE:DOTAP) provides an absorbed dose profile that follows the cell density profile better than SUV (DMPC-chol); the MLV system remains optimal for a cell-density–based distribution.

The earlier discussion and the modeling analysis presented in this work are limited to micrometastases that do not present with a central vessel but, rather, peripheral vessels. In the case of a central vessel model, both high cell density and hypoxia would be observed at the periphery. The appropriate radionuclide and liposomal penetration characterictics in this situation would be different. It is important to note that the results presented here represent an idealized scenario, chosen to investigate the inherent tumor penetration characteristics and resulting radionuclide and absorbed dose distributions of different liposomal constructs. Actual absorbed dose distributions will be influenced by the half-life of the radionuclide and by the uptake and clearance kinetics of liposomal constructs in the circulation. Liposomal delivery of radionuclides offers several potential advantages relative to molecular (antibody or peptide based) delivery. The structure of liposomes could allow for the delivery of larger amounts of radioactivity, increasing the specific activity per delivered particle. Alternatively, the incorporation of different radionuclides with different half-lives, emission types, and ranges could be envisioned (*21*). Correspondingly, liposomes could be coated with different targeting moieties, thereby targeting several different antigens and reducing possible escape of tumor cells not expressing a particular antigen. Coating of liposomes with binding moieties raises the potential for inhibiting penetration by a binding-site mechanism (*35–37*). Given the potential complexity of such an approach, studies performed, in vitro, of the type described in this article will be essential in establishing a foundation for the eventual clinical implementation of liposome-mediated targeted radionuclide therapy.

CONCLUSION

A dosimetric analysis of the absorbed dose distribution within a tumor spheroid model for clinically relevant liposome systems and for the antibody J591 has been performed for a variety of electron-emitting radionuclides. The results suggest that it is possible to engineer liposome systems that are particularly effective in irradiating the central core region of the tumor, provided that conjugates with the appropriate radionuclides are constructed. Also, liposomes may effectively complement an antibody-based therapeutic regime against micrometastatic tumors, leading to an absorbed dose profile that can match the desired optimal profile throughout the tumor mass.

ACKNOWLEDGMENTS

Digital imaging and microscopy were performed at the Molecular Cytology Core Facility, Memorial Sloan-Kettering Institute, New York, NY, with assistance from Dr. Katia Manova. The authors thank Dr. Neil Bander of the Weill Cornell Medical College for supplying the J591 antibody. This work was supported, in part, by National Institutes of Health grants R01 CA62444 and R01 CA72683, by U.S. Army grant DAMD17-0010657, and also by the University of Ioannina Committee of Research grant 62/1293.

REFERENCES

1. Allen TM. Ligand-targeted therapeutics in anticancer therapy. *Nat Rev Cancer.* 2002;2:750–763.

2. Gabizon AA. Liposomal drug carrier systems in cancer chemotherapy: current status and future prospects. *J Drug Target.* 2002;10:535–538.
3. Emfietzoglou D, Kostarelos K, Sgouros G. An analytic dosimetry study for the use of radionuclide-liposome conjugates in internal radiotherapy. *J Nucl Med.* 2001;42:499–504.
4. Makrigiorgos GM, Ito S, Baranowska-Kortylewicz J, et al. Inhomogeneous deposition of radiopharmaceuticals at the cellular level: experimental evidence and dosimetric implications. *J Nucl Med.* 1990;31:1358–1363.
5. Sgouros G. Radiolabeled antibodies: overview. In: Bertino J, ed. *Encyclopedia of Cancer.* New York, NY: Academic Press; 2002:29–40.
6. Sgouros G. Radioimmunotherapy of micrometastases. In: Riva P, ed. *Cancer Radioimmunotherapy: Present and Future.* Amsterdam, The Netherlands: Harwood Academic Publishers; 1998:191–207.
7. Sgouros G. Radioimmunotherapy of micrometastases: sidestepping the solid-tumor hurdle. *J Nucl Med.* 1995;36:1910–1912.
8. Humm JL, Cobb LM. Nonuniformity of tumor dose in radioimmunotherapy. *J Nucl Med.* 1990;31:75–83.
9. Meredith RF, Johnson TK, Plott G, et al. Dosimetry of solid tumors. *Med Phys.* 1993;20:583–592.
10. O'Donoghue JA, Bardies M, Wheldon TE. Relationships between tumor size and curability for uniformly targeted therapy with beta-emitting radionuclides. *J Nucl Med.* 1995;36:1902–1909.
11. Goddu SM, Rao DV, Howell RW. Multicellular dosimetry for micrometastases: dependence of self-dose versus cross-dose to cell nuclei on type and energy of radiation and subcellular distribution of radionuclides. *J Nucl Med.* 1994;35:521–530.
12. O'Donoghue JA. Implications of nonuniform tumor doses for radioimmunotherapy. *J Nucl Med.* 1999;40:1337–1341.
13. Ballangrud AM, Yang WH, Charlton DE, et al. Response of LNCaP spheroids after treatment with an α-particle emitter (^{213}Bi)-labeled anti-prostate-specific membrane antigen antibody (J591). *Cancer Res.* 2001;61:2008–2014.
14. Ballangrud AM, Yang WH, Dnistrian A, Lampen NM, Sgouros G. Growth and characterization of LNCaP prostate cancer cell spheroids. *Clin Cancer Res.* 1999;5:3171s–3176s.
15. Buffa FM, West C, Byrne K, Moore JV, Nahum AE. Radiation response and cure rate of human colon adenocarcinoma spheroids of different size: the significance of hypoxia on tumor control modelling. *Int J Radiat Oncol Biol Phys.* 2001;49:1109–1118.
16. Essand M, Gronvik C, Hartman T, Carlsson J. Radioimmunotherapy of prostatic adenocarcinomas: effects of ^{131}I-labelled E4 antibodies on cells at different depth in DU 145 spheroids. *Int J Cancer.* 1995;63:387–394.
17. van Leeuwen-Stok AE, Schuurhuis GJ, Drager A, et al. Radiotoxic effect and dosimetry of ^{67}Ga in multicellular spheroids as compared to single cells of the lymphoma cell line U715. *Int J Radiat Oncol Biol Phys.* 1996;35:507–517.
18. Weber W, Weber J, Senekowitsch-Schmidtke R. Therapeutic effect of m-[^{131}I]- and m-[^{125}I]iodobenzylguanidine on neuroblastoma multicellular tumor spheroids of different sizes. *Cancer Res.* 1996;56:5428–5434.
19. McDevitt MR, Barendswaard E, Ma D, et al. An α-particle emitting bismuth-213 labeled antibody (J591) to the external domain of prostate specific membrane antigen. *Cancer Res.* 2000;60:6095–6100.
20. Kostarelos K, Emfietzoglou D. Tissue dosimetry of liposome-radionuclide complexes for internal radiotherapy: toward liposome-targeted therapeutic radiopharmaceuticals. *Anticancer Res.* 2000;20:3339–3345.
21. Sofou S, Thomas JL, Lin H, McDevitt MR, Scheinberg DA, Sgouros G. Engineered liposomes for potential α-particle therapy of metastatic cancer. *J Nucl Med.* 2004;45:253–260.
22. Yuhas JM, Li AP, Martinez AO, Ladman AJ. A simplified method for production and growth of multicellular tumor spheroids. *Cancer Res.* 1977;37:3639–3643.
23. Mui BL, Cullis PR, Evans EA, Madden TD. Osmotic properties of large unilamellar vesicles prepared by extrusion. *Biophys J.* 1993;64:443–453.
24. Litzinger DC, Buiting AM, van Rooijen N, Huang L. Effect of liposome size on the circulation time and intraorgan distribution of amphipathic poly(ethylene glycol) containing liposomes. *Biochim Biophys Acta.* 1994;1190:99–107.
25. Liu H, Moy P, Kim S, et al. Monoclonal antibodies to the extracellular domain of prostate-specific membrane antigen also react with tumor vascular endothelium. *Cancer Res.* 1997;57:3629–3634.
26. Liu H, Rajasekaran A, Moy P, et al. Constitutive and antibody-induced internalization of prostate-specific membrane antigen. *Cancer Res.* 1998;58:4055–4060.
27. Mason DW, Williams AF. The kinetics of antibody binding to membrane antigens in solution and at cell surface. *Biochem J.* 1980;187:1–20.
28. Silver DA, Pellicer I, Fair WR, Heston WD, Cordon-Cardo C. Prostate-specific membrane antigen expression in normal and malignant human tissues. *Clin Cancer Res.* 1997;3:81–85.
29. Howell RW, Rao DV, Sastry KSR. Macroscopic dosimetry for radioimmunotherapy: nonuniform activity distributions in solid tumors. *Med Phys.* 1989;16:66–74.
30. Cross WG, Ing H, Freedman N. A short atlas of beta ray spectra. *Phys Med Biol.* 1983;28:1251–1260.
31. Cole A. Absorption of 20 eV to 50000 eV electron beams in air and plastic. *Radiat Res.* 1969;38:7–33.
32. Attix FH. *Introduction to Radiological Physics and Radiation Dosimetry.* New York, NY: John Wiley & Sons; 1986.
33. Humm JL. Dosimetric aspects of radiolabeled antibodies for tumor therapy. *J Nucl Med.* 1986;27:1490–1497.
34. Hill RP, Pallavicini MG. Hypoxia and the radiation response of tumors. *Adv Exp Med Biol.* 1981;159:17–35.
35. van Osdol W, Fujimori K, Weinstein JN. An analysis of monoclonal antibody distribution in microscopic tumor nodules: consequences of a "binding site barrier." *Cancer Res.* 1991;51:4776–4784.
36. Sgouros G. Plasmapheresis in radioimmunotherapy of micrometastases: a mathematical modeling and dosimetrical analysis. *J Nucl Med.* 1992;33:2167–2179.
37. Saga T, Neumann RD, Heya T, et al. Targeting cancer micrometastases with monoclonal antibodies: a binding-site barrier. *Proc Natl Acad Sci USA.* 1995;92:8999–9003.